CMST 31(4) 107–119 (2025) DOI:10.12921/cmst.2025.0000019

Elastic properties of the f.c.c. hard sphere crystal with thick nanolayer-nanochannel inclusions formed by hard dumbbells

J.W. Narojczyk[1*], **K.V. Tretiakov**[1,2], **K. W. Wojciechowski**[1]

[1] *Institute of Molecular Physics, Polish Academy of Sciences*
M. Smoluchowskiego 17,
60-179 Poznań, Poland
E-mail: narojczyk@ifmpan.poznan.pl

[2] *President Stanisław Wojciechowski University of Kalisz*
Polytechnic Faculty
Nowy Świat 4,
62-800 Kalisz, Poland

Received: 14 October 2025; accepted: 8 December 2025

Abstract: The article investigates the possibility of modifying the elastic properties of materials by altering their structure at the atomic level. Such approach could prove useful in tailoring the properties of materials to particular applications. Advances in the nano-level techniques may prove this approach to be a cost-effective and fast to implement method of achieving this goal. The subject of this work are studies of elastic properties of f.c.c. crystals with inclusions containing di-atomic molecules, forming aperiodic phase within these inclusions. Recent studies showed that such phase may enhance auxetic properties of the crystal. It has been discovered that Poisson's ratio in the direction of $[110]$ has been decreased from -0.054 (pure f.c.c. crystal) down to -0.235 (inclusions with aperiodic phase of dumbbells). Here, different sized of the inclusions are investigated, in order to extend that study. It has been found that increasing the size of the inclusions will completely eliminate the auxetic properties when the diameters of the inclusion spheres increase. However, the decreasing atomic diameters show that auxetic properties can be switched between the in-plane and out-of-plane directions (with respect to inclusion nanolayers), by rotating the shape of the nanochannel around its longitudinal axis.

Key words: auxetics, degenerate phase, elastic properties, hard dumbbells, hard spheres, nanoinclusions, Poisson's ratio

I. Introduction

Negative Poisson's ratio [1] materials, although theoretically possible, have not been known to exist until the late 1980s. Many believed that such properties of materials are not possible in reality. It was the two ground braking works that had changed the mindset of researchers and started a completely new area of research that is rapidly evolving to this day. One of the works showed that such materials can exist, by making a specially heat-treated foam [2], that exhibit negative Poisson's ratio. The other one focused on the simple thermodynamic model systems of hard cyclic hexamer molecules in 2D [3], and proved, by its rigorous solution in the static (zero temperature) limit [4], that it is possible to obtain a thermodynamicaly stable system exhibiting a negative Poisson's ratio. *Auxetic* [5] materials, as they came to be called, exhibit a whole range of counter-intuitive mechanical properties. Among others, their most famous property is to expand laterally while subjected to longitudinal stretching. Such extraordinary properties [6–8] and their vast potential applications [9–12], drive the motivation of the ever-growing number of researchers to deepen our knowledge

and understanding of the physical phenomena behind these elastic properties. Auxetics have been extensively studied from the macroscopic perspective. The studies concentrate on auxetic structures [13–20], foams [21–24], fabrics [25–27], and composites [28–31]. The studies on auxetic metamaterials [32–36] constitute a step towards the analysis on the micro level. In parallel, theoretical investigations have been done to formulate various macro [13] or scale independent models [37–44] that show these properties. Another approach to this subject is to look for the origin of the auxetic properties at the micro or atomic levels. It has been found that about 69% of crystals with cubic symmetry exhibit auxeticity [45]. The reason why these observations have not been made earlier is that the negative Poisson's ratio occurs in these crystals only in the narow range of crystalographic directions, whereas in other ones the PR is positive. Such materials are now called *partial auxetics* [46]. A number of atomic models have been proposed to examine the nature of auxeticity in materials [47–51]. These and many other studies have shown that modifying the atomic structure of materials is a feasible approach to modify macroscopic elastic properties of the material. Possibly to enhance its auxetic properties to match the intended application. However, this is a cumbersome task, as our understanding of how the processes that occur on the atomic level, translate to the macroscopic properties of materials is still limited. Thus, further studies of simple atomic models are required. One of the proposed directions of study is modification of the crystalline structure with inclusions. Although models described here are purely theoretical, the advances in nanotechnology to date, allow us to fabricate systems even with monoatomic layers [52]. Thus, insight provided by such models may prove valuable while designing and creating microscale sensors or actuators in MEMS systems.

Nanolevel inclusions to crystalline structure is one approach towards modification of elastic properties of crystals [53]. Such inclusions may be implemented in various shapes and forms. Recently, a model has been proposed, where in f.c.c. crystal of hard spheres certain spheres have been replaced by hard spheres of different diameters. The included spheres have been arranged in the form of an array of $[001]$-nanochannels [54]. When the diameters of these include spheres increased above 8% over the remaining spheres in the system, a strong enhancement of the auxetic properties have been observed. Yet, similar studies with inclusion in the form of a periodic stack of (001) crystalographic mono-layers showed only slight enhancement of the auxeticity [55]. However, the most surprising result was obtained when both types of inclusions have been implemented in a single model. It has been found that inclusion in such a form completely eliminates the auxetic properties of the f.c.c. crystal of hard spheres [56]. This shows that processes on atomic level do not translate to macroscopic properties in a simple manner, and the observed effects are not additive. Lately, these studies have been extended by introducing additional constrains on spheres forming inclusions. The latter have been randomly paired to form simple di-atomic molecules, the dumbbells. The study of a model with (001)-nanolayers joined with thin $[001]$-nanochannels, filled with dumbbell molecules showed that auxetic properties can occur in such a model, and can be strongly enhanced, compared to pure f.c.c. hard sphere crystal [57]. The molecules within the inclusion form the so-called *Degenerate Crystalline* (DC) phase [58, 59], an aperiodic phase [60], featuring no translational nor rotational order of molecules. Recently this study has been further extended, to investigate the impact of increasing number of adjacent (001)-nanolayers or the widening of the $[001]$-nanochannels [61] The study showed that increasing the number of layers and/or the thickness of nanochannels, one can completely eliminate or decrease the auxetic properties , respectively.

The aim of the current study is to extend that research by studying models containing arrays of wider $[001]$-nanochannels joined with the stacks of multiple (two or three) adjacent (001)-nanolayers, filled by the dumbbell molecules forming the DC phase. Along with the previous studies, these models will increase our understanding of the impact of changing atomic sizes in the presence of molecular bonds as well as different sizes and geometries of inclusions, on elastic properties.

II. Studied systems

The models examined in this work are based on an f.c.c. crystal composed of N hard spheres in periodic boundary conditions. In the uniform (monodisperse) crystal each sphere has the diameter of σ, which is also considered as the unit of length. To such a crystal, inclusions with spheres of different diameter ($\sigma' \neq \sigma$) are introduced. This is obtained by replacing selected spheres from the pristine crystal (*the matrix*) with inclusion spheres. All the latter spheres have the same diameter. Thus, one obtains a binary system composed of hard spheres either of the diameter σ' (counting N_{inc} spheres) or σ (counting $N - N_{\text{inc}}$ spheres). The ratio of the number of inclusion spheres to the number of all the spheres in the system (N_{inc}/N) is referred to as *the concentration*. The number of inclusion spheres and their spacial localization is arbitrary. Thus, one can introduce inclusion of various shapes and sizes. In this work, we focus on models with joined nanochannel and nanolayer inclusions. Here, we introduce nanolayers in the form of two (L2) or three (L3) adjacent (001) crystallographic layers, stacked periodically along the $[001]$-direction. The nanolayers are joined with an array of orthogonal nanochannels, oriented along $[001]$-direction. The array is periodically stretched in x-y plane. The diameters of the introduced nanochannels are such to encompass spheres in the second (C2) and third (C3) coordination zone from the channel's axis. This corresponds to the nanochannel radii equal to σ and $\sqrt{2}\sigma$ respectively. The four possible combinations of the proposed inclusions are presented in Figure 1a). These models will be further referenced to as CiLj, where $i, j = 2, 3$. After the inclusions have been introduced into the crystal, additional constrains are imposed on the inclusion spheres. They are randomly connected into di-atomic molecules (*dumbbells*). The latter are rigid and their length l is equal to σ, i.e. the centres of spheres forming a dumbbell are separated by the distance of

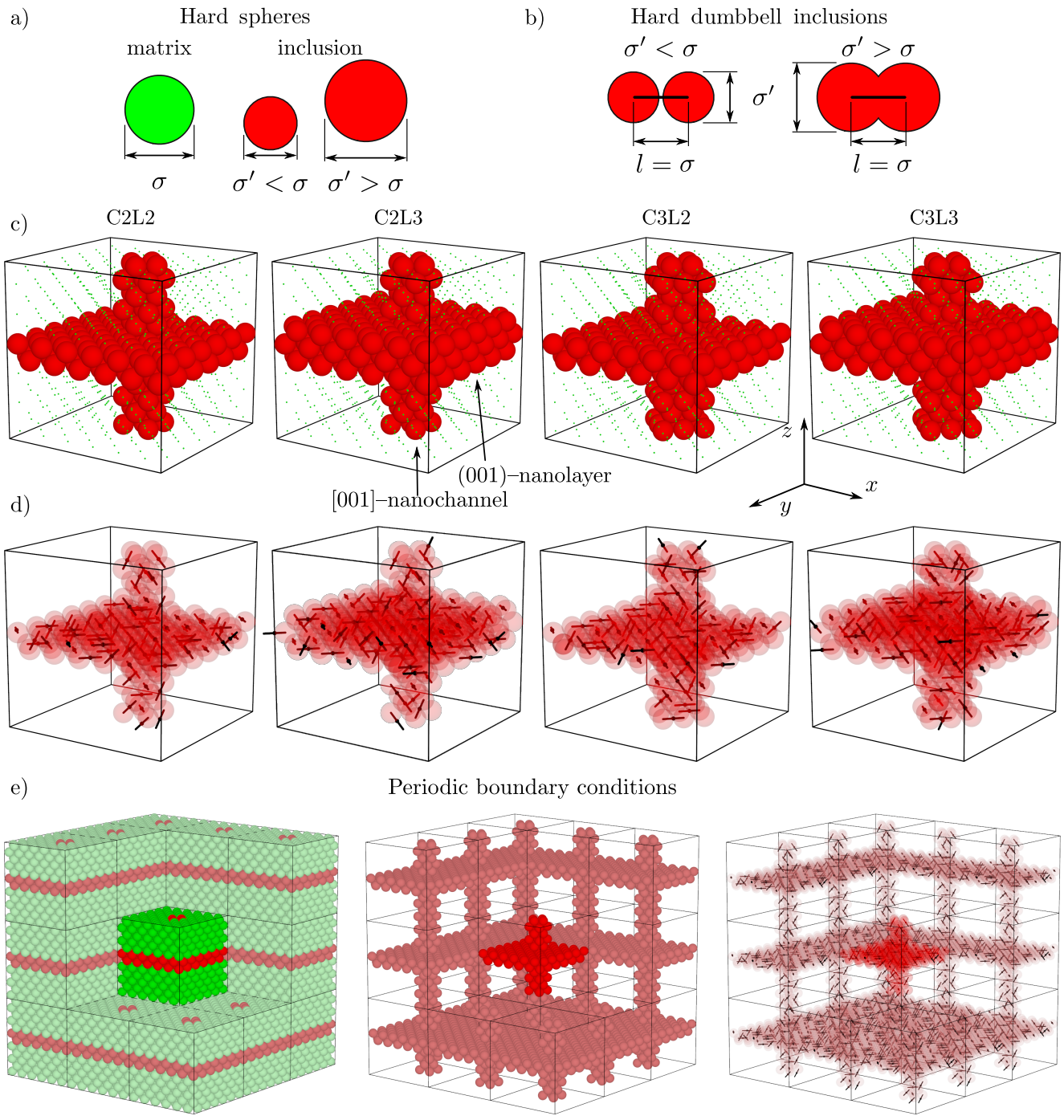

Fig. 1. Visualization of a) atomic inclusions to the f.c.c. structure, b) pairing of the atomic inclusion spheres into dumbbell molecules, c) studied topologies of inclusions of different number of adjacent nanolayers and various sizes of nanochannels (shown as atomic systems). The small green spheres in c) represent the matrix spheres, which were artificially scaled down, only for the viewing purposes. In d) one of many possible arrangement of dumbbell molecules within the inclusion is presented (the matrix spheres have been artificially removed). Part e) presents the studied supercell of C2L2 system in periodic boundary conditions. In the latter part, some periodic images of the supercell have been removed to facilitate the view.

σ, regardless of the diameters of the individual spheres (see Fig. 1b). At close packing, the dumbbells can be oriented along six different directions, namely: [110], [1$\bar{1}$0], [101], [10$\bar{1}$], [011], and [01$\bar{1}$]. The random pairing of the inclusion spheres results in a phase that does not exhibit any periodic order of molecules. Thus, this phase is a representation of the DC phase of dumbbells within an f.c.c. lattice. The visualization of the periodic supercell with molecular bonds

is presented in Fig. 1c), where matrix spheres were removed and the inclusion spheres have been shown semi-transparent, to reveal the distribution of molecules. The example supercell for C2L2 system have been shown with some of its periodic images in Fig. 1d).

All spheres in the system interact *via* a (purely geometrical) hard potential, which can be expressed in the form:

$$\beta u_{ij} = \begin{cases} \infty, & r_{ij} < \sigma_{ij}, \\ 0\ , & r_{ij} \geq \sigma_{ij}, \end{cases} \tag{1}$$

where r_{ij} is the distance between the centres of spheres i and j, and σ_{ij} represents the sum of their radii. β equals $1/(k_{\mathrm{B}}T)$, where k_{B} is the Boltzmann constant and T is the temperature. The total energy of the system is $U = (\beta/2) \cdot \Sigma_{ij}^{'} u_{ij}$, where $\Sigma_{ij}^{'} u_{ij}$ represents a double sum with the condition $i \neq j$. Because the molecules in the inclusion are considered rigid ($l = \sigma = \mathrm{const}$), the interaction between inclusion spheres within a dimer is excluded from calculations, i.e. does not contribute to the total energy of the system. The hard sphere interaction potential is used as the fundamental reference model in the condensed matter physics [62, 63] and, what is important for the current study, a hard sphere crystal exhibits a negative Poisson's ratio [64, 65] and can be thought of as a partial auxetic [46].

III. Methods

III. 1. Elastic Properties

The computer simulations have been used to determine the elastic properties of the proposed models. Simulations were done by Monte Carlo (MC) method implementing the Parrinello–Rahman approach [66–68]. This method allows one to calculate the full elastic compliance tensor for the crystal, through a single run in the isobaric–isothermal ensemble (NpT). The studied supercell occupies the parallelepiped space that can be described by the so-called box matrix ($\mathbf{h}$), a symmetric square matrix of the rank three. It is composed of the vectors defining edges of the parallelepiped. This parallelepiped changes over the course of the simulation. Hence, the $\mathbf{h}$ matrix also changes. As shown in Ref. [67], one can express the Lagrange strain tensor as function of the box matrix and the reference box matrix ($\mathbf{h}_{\mathrm{p}}$), in the following form:

$$\boldsymbol{\varepsilon} = \frac{1}{2}\left(\mathbf{h}_{\mathrm{p}}^{-1}.\mathbf{h}.\mathbf{h}.\mathbf{h}_{\mathrm{p}}^{-1} - \mathbf{I}\right)\ , \tag{2}$$

where $\mathbf{I}$ is the identity matrix. The reference box matrix $\mathbf{h}_{\mathrm{p}} \equiv \langle \mathbf{h} \rangle$ is the (ensemble) average value of the $\mathbf{h}$ matrix at equilibrium under *dimensionless* pressure $p^* = p\beta\sigma^3$. The components of the Lagrange strain tensor $\boldsymbol{\varepsilon}$ allow one to calculate the elastic compliance tensor, defined as [68]:

$$S_{\alpha\beta\gamma\delta} = \beta V_{\mathrm{p}} \left\langle \Delta\varepsilon_{\alpha\beta} \Delta\varepsilon_{\gamma\delta} \right\rangle\ . \tag{3}$$

In the above equation, $V_{\mathrm{p}} = |\det(\mathbf{h}_{\mathrm{p}})|$ is the average volume of the system at the dimensionless pressure p^* and $\Delta\varepsilon_{\alpha\beta} = \varepsilon_{\alpha\beta} - \langle\varepsilon_{\alpha\beta}\rangle$, whereas the $\langle\varepsilon_{\alpha\beta}\rangle$ is the average of the components of the strain tensor in the NpT ensemble, and $\alpha, \beta, \gamma, \delta$ = x, y or z. The elastic compliance tensor S is a symmetric fourth-rank tensor, that allows one to describe in full the elastic properties of the crystal at any symmetry. Often it is more convenient to analyse elastic properties in terms of elastic constants rather than elastic compliances. The latter tensor can be also easily obtained from the following relation [69]:

$$\sum_{n,m} S_{ijmn} B_{mnkl} = \frac{1}{2}\left(\delta_{ik}\delta_{jl} + \delta_{il}\delta_{jk}\right)\ , \tag{4}$$

where δ_{ij} is the Kronecker delta. As mentioned above, the knowledge of the elastic compliance tensor S allows one for complete description of a crystal's elastic properties. Specifically, the Poisson's ratio in any direction can be determined using the expression [70]:

$$\nu_{nm} = -\frac{m_\alpha m_\beta S_{\alpha\beta\gamma\delta} n_\gamma n_\delta}{n_\zeta n_\eta S_{\zeta\eta\kappa\lambda} n_\kappa n_\lambda}\ . \tag{5}$$

From the above, it's evident that PR depends on two mutually orthogonal directions, represented by the unit vectors $\vec{\mathbf{n}}$ and $\vec{\mathbf{m}}$. The former indicates the direction of the applied external stress, while the latter ($\vec{\mathbf{m}}$) represents the direction in which the PR is measured. It should also be noted that the Einstein summation convention is used for Greek indices. For clarity, in the rest of the manuscript, we express the $S_{\alpha\beta\gamma\delta}$ and $B_{\alpha\beta\gamma\delta}$ tensor elements in terms of the elastic compliance matrix S_{ij} and the elastic constant matrix B_{ij} elements, respectively, using Voigt notation [71]. The Latin indices for the S_{ij} and B_{ij} elements of this symmetric square matrix take the values $i, j = 1, ..., 6$. The described approach pertains to infinitesimally small deformations. If this had not been the case, a different approach should have ben used, e.g., the one described in [3].

III. 2. Computational Details

Monte Carlo simulations done in this work used the standard Metropolis algorithm [63] with two types of trial moves. The first type changed the particles' position and/or orientation of dumbbells, and the second type was responsible for the changes of the system shape (the change of the box matrix $\mathbf{h}$). During a single MC cycle an attempt to move (and/or rotate) each particle once, has been performed. Attempts to change the box matrix components have been performed every $\sqrt{N}$ particle trial moves. The acceptance ratio for both types of trial moves has been set to 40%. Single simulation run took 10^7 MC cycles, of which the initial 10% has been treated as period when system reached thermodynamic equilibrium, and were discarded from simulations.

Models with $N = 864$, that correspond to crystal of $6 \times 6 \times 6$ f.c.c. unit cells, have been examined. Depending on the model, inclusions contained $N_{\mathrm{inc}} = 189$ spheres for C2L2, $N_{\mathrm{inc}} = 257$ spheres for C2L3, $N_{\mathrm{inc}} = 209$ spheres for C3L2, and $N_{\mathrm{inc}} = 277$ spheres for C3L3. Thus, the concentration of inclusion spheres in the given systems was $c = 21.875\%$, 29.75%, 24.19%, and 32.06%, respectively.

All systems were subjected to the external dimensionless pressure $p^* = 100$. The impact of changes of the inclusion sphere diameters was investigated in the range of σ'/σ from 0.95 to 1.05. The selected σ' had not changed during a simulation run. For each value of σ' five hundred individual simulations have been performed and the values of elastic compliance matrix have been averaged prior to Poisson's ratio calculations.

IV. Results and Discussion

Earlier studies [56] have shown, that introduction of hybrid nanolayer-nanochannel inclusion into an f.c.c. crystal lowers the symmetry of the system from cubic to tetragonal one [71]. Similarly, in the current study, presented results concern only the range of parameters (p^*, σ') for which the stable tetragonal phase has been obtained. To confirm the symmetry of systems obtained from simulations one must examine their shapes and their elastic compliances. In Figure 2 the values of the diagonal box matrix components are presented for the C2 (a) and C3 (b) size nanochannels, respectively. The data for systems with two adjacent nanolayers (L2) have been plotted in orange and the data concerning L3 systems, with black. It can be observed that, similarly to [56], the in-plane dimensions, with respect to the inclusion layer, are equal for systems at their respective σ'/σ values, i.e. $h_{11} = h_{22}$ for each model. The values of h_{11} and h_{22} increase with the increase of σ'/σ to accommodate for the increase of inclusions. However, this increase in x and y dimensions allows for the compression in z-directions, what is reflected by the h_{33} values in all systems. These values are lower for both L2 systems, as the increase of σ'/σ affects the thickness of only two crystallographic layers. The increase of the in-plane dimensions at high σ'/σ allows to compress the crystal in [001] direction even below the value of the pristine f.c.c. sample. The reason behind this contraction is mainly due to the fact that matrix spheres have more available space to expand in x-y directions. When diameters of inclusion spheres decrease ($\sigma'/\sigma < 1$), one can observe a similar contraction of all systems. However, in this case the mechanism is different. The joined inclusion layers as well as the channel length decrease in z-direction, hence the resulting compression is greater for L3 systems. Only minor contraction observed on h_{11} and h_{22} is due to the matrix of the crystal, which cannot be compressed any further when σ'/σ is decreased below 0.99.

In Figure 3 the selected elements of the elastic compliance matrix S^*_{ij} are presented. The data corresponding to thinner (C2) nanochannel systems have been plotted with open symbols and the ones corresponding to wider (C3) nanochannel, with closed symbols, respectively. Furthermore, the data for two adjacent nanolayer systems (L2) have been indicated with circles, and the L3 systems have been represented by triangle symbols. As mentioned in Section III. 1. elastic compliance matrix **S** has 36 elements. Due to the symmetry of the matrix, only 21 elements are enough to describe the crystal at the lowest possible symmetry. For cubic symmetry the number of independent elastic compliance elements is down to only S_{11}, S_{12}, and S_{44}, while the remaining elements are zero. As it can be seen in Fig 3, in this case there are six independent elastic compliance elements, while the remaining ones are zero (to the degree of computational accuracy). Thus, the matrix of elastic compliance takes the form:

$$\mathbf{S} = \begin{bmatrix} S_{11} & S_{12} & S_{13} & 0 & 0 & 0 \\ S_{12} & S_{11} & S_{13} & 0 & 0 & 0 \\ S_{13} & S_{13} & S_{33} & 0 & 0 & 0 \\ 0 & 0 & 0 & S_{44} & 0 & 0 \\ 0 & 0 & 0 & 0 & S_{44} & 0 \\ 0 & 0 & 0 & 0 & 0 & S_{66} \end{bmatrix}. \quad (6)$$

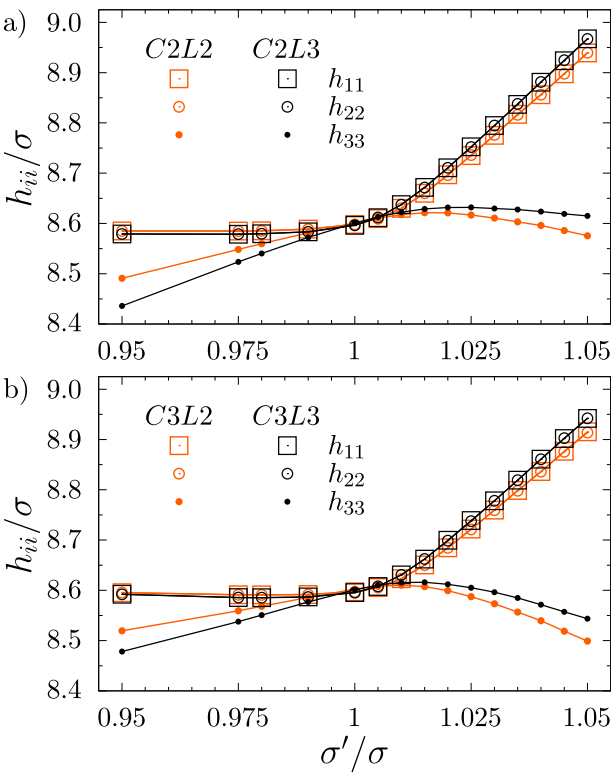

Fig. 2. The diagonal elements of the box matrix **h** for C2 (a) and C3 (b) models.

This confirms that, as in earlier studies of similar inclusion without dumbbells [56], the symmetry of the resulting systems is the tetragonal one (422 symmetry class [71]). The following conditions, that are required for the tetragoanal symmetry are met:

$$\begin{aligned} S_{11} &= S_{22}, \\ S_{13} &= S_{23}, \\ S_{44} &= S_{55}, \\ S_{i4} &= S_{i5} = S_{i6} = 0 \text{ for } i = 1, 2, 3, \\ S_{45} &= S_{46} = S_{56} = 0. \end{aligned} \quad (7)$$

The plots in Fig. 3 have been arranged such, that the columns represent pairs of elastic compliances that are equal to each other in the cubic case. An important remark is required here, as when $\sigma'/\sigma = 1$ all the spheres' diameters in the system

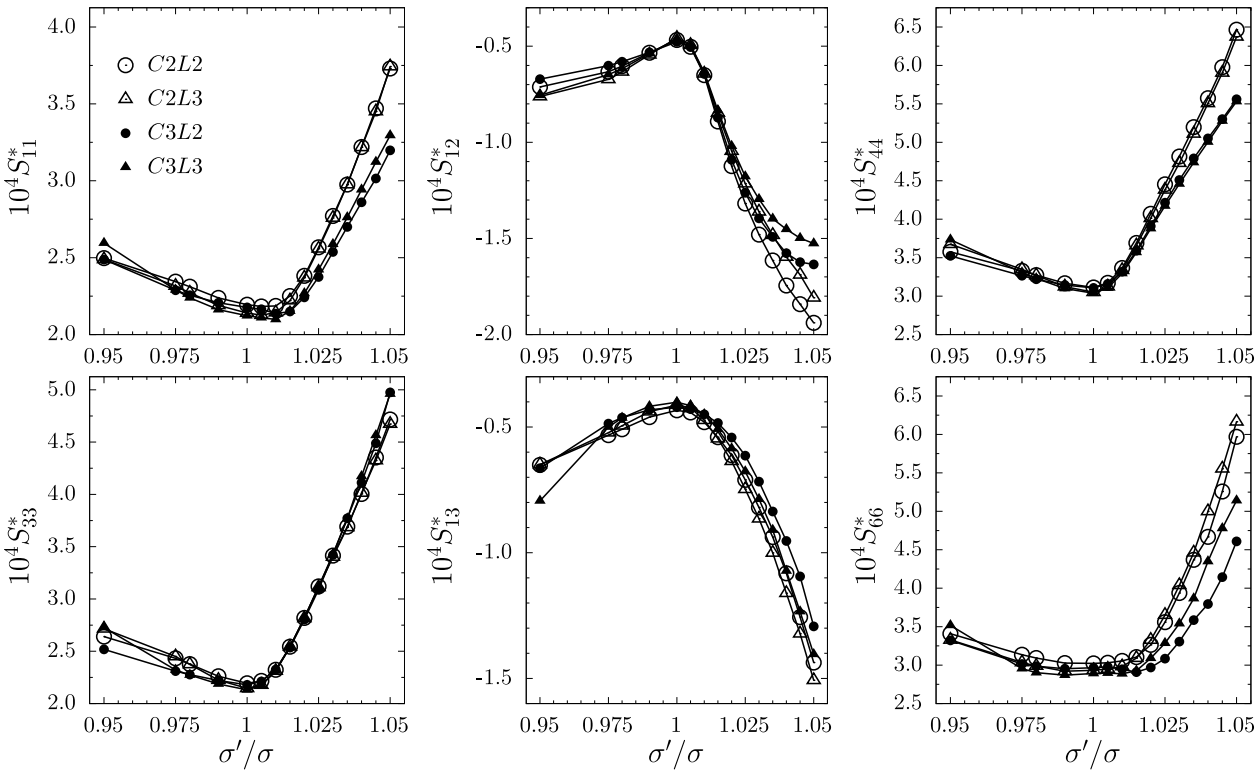

Fig. 3. The elastic compliance matrix elements (S^*_{ij}) for all studied models.

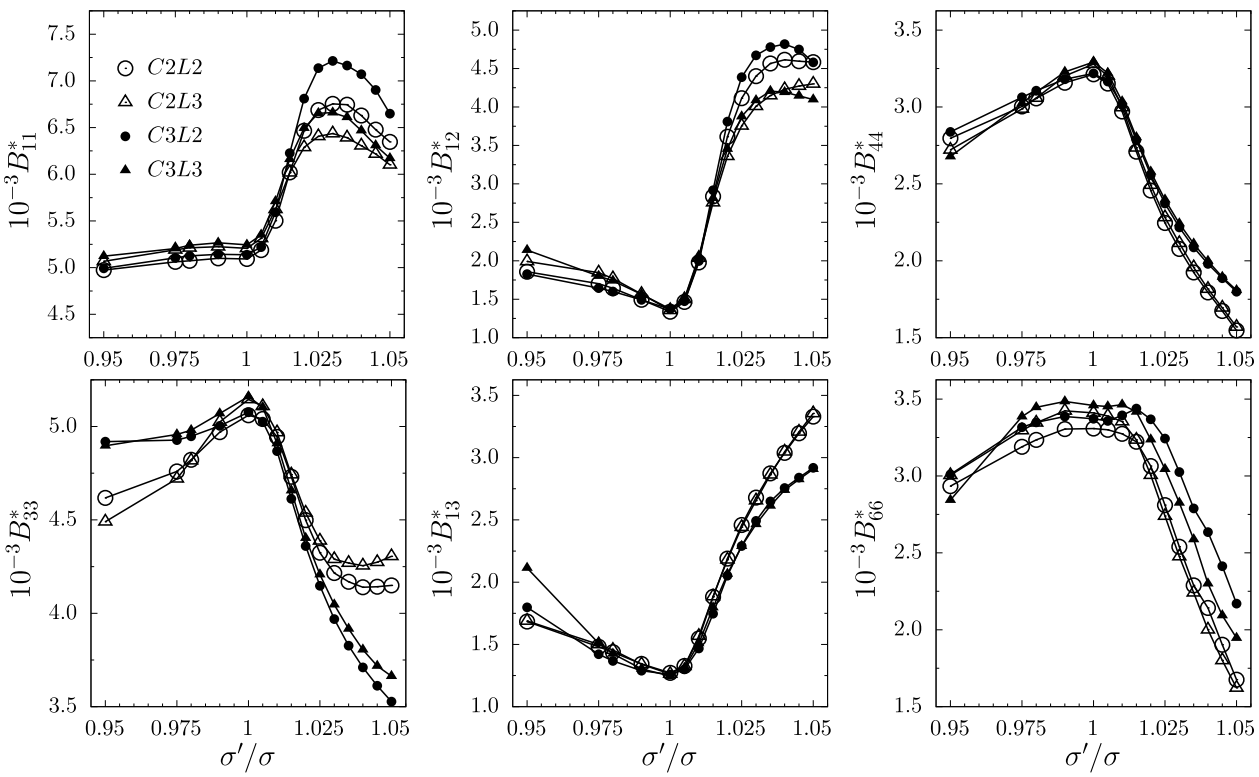

Fig. 4. Elements of the elastic constants matrix (B^*_{ij}) for all studied models.

are equal and, at close packing, one obtains systems, where all the spheres form the perfect f.c.c. crystal. However, one should keep in mind that the presence of molecular bonds within the inclusion breaks the symmetry of the crystal even at $\sigma'/\sigma = 1$ and there is not even a single case in this study, where the symmetry of the system is cubic. It can be seen from the plots that, qualitatively, all studied systems react the same to the changes of atomic diameters of inclusion spheres (σ'/σ). S^*_{12} and S^*_{13} decrease, regardless of whether $\sigma'/\sigma < 1$ or $\sigma'/\sigma > 1$. All the remaining four compliance elements increase when $\sigma'/\sigma \neq 1$. The increase, however, is more significant when atomic diameter of inclusion particles become larger. Interestingly, S^*_{33} values for all studied models are very close, suggesting its low dependence on the concentration of inclusion particles, which changes from 21% to 32% (see Sec. III. 2.). The S^*_{11}, S^*_{44}, and S^*_{66} elements, however, show that the elastic compliance of models with thinner nanochannels (C2) increases over the wider nanochannel systems, regardless of the number of adjacent nanolayers introduced. Based on the S^*_{11}, S^*_{12}, and S^*_{66}, one can conclude that typically the L3 systems have higher value of the elastic compliance over the L2 systems, regardless of the nanochannel diameter.

In Figure 4 values of elastic constants matrix $\mathbf{B}$, calculated as described by Eq. (4), have been presented, per analogy to Fig. 3. It should be also noted, that elastic constants B_{ij} also follow the relations given in Eq. (8). It can be noticed from the B^*_{11} and B^*_{33} plots, that the resistance to compression in x-y plane is significantly increased due to the presence of molecular inclusions and increased atomic sizes. Whereas, compression resistance in the z-direction (B^*_{33}) for all models decreases along with the increase of σ'/σ. The reason behind this is an obvious consequence of the changes in the sample's shape, described above in the discussion of Fig. 2. The presence of molecular bonds within the inclusion layers are primarily responsible for the increase in compression resistance in-plane directions. Whereas, the in-plane expansion of the crystal weakens the out-of-plane compression resistance. Surprisingly, L2 systems have higher values of B^*_{11} compared to L3 systems, and despite the fact that the number of adjacent inclusion layers is a key factor in this regard, the wider nanochannel systems (C3) exhibit higher compression resistance over the respective C2 counterparts. When comparing the compression resistance in the z-direction, the C2L3 system exhibits the highest value of B^*_{33}. Following the analysis of elastic compliance, here also one might notice on B^*_{44} and B^*_{66}, that shear resistance is lowered in almost every case when $\sigma'/\sigma \neq 1$. It can be noticed that the in-plane shear resistance is the highest for C3L2 model at high values of σ'/σ. However, this changes when atomic diameters drop below $\sigma'/\sigma = 1.015$, when C3L3 is the most resistant to shear deformations in x, y plane. Similar to what was observed on elastic compliance plots, values of B^*_{13} show minor dependence on the number of adjacent nanolayers. In case of this value, the key factor is the width of the nanochannel. Whereas, B^*_{12} constants depend rather on the number of nanolayers, especially at high values of σ'/σ.

In Figure 5 the Poisson's ratio (ν_{nm}) in selected crystallographic directions has been presented, plotted as the function of σ'/σ. The directions n, m indicate the loading direction and the direction of measurement, respectively. In general, it can be observed that changing the atomic diameters of the inclusion particles results in the increase of PR every case among the eight selected directions. The changes of Poisson's ratio are more significant then the inclusion sphere diameters increase ($\sigma'/\sigma > 1$). It can be noticed, that in most of the presented directions, the values of PR depend rather on the diameter of the nanochannel, rather than on the number of the adjacent nanolayer. In the case of $\nu_{[101]}$, $\nu_{[111]}$, and $\nu_{[110][1\bar{1}0]}$ the wider the nanochannel leads to the smaller the value of Poisson's ratio. Whereas, PR for models with different L-number but the same respective nanochannel size, have very similar values. This is especially apparent for $\nu_{[101][\bar{1}01]}$, where the C2 systems show high increase of PR value when σ'/σ increases. For the corresponding values of σ'/σ, the C3 systems exhibit PR very close to zero. Only in the case of $\nu_{[100][010]}$ one can notice a clear dependence on the number of adjacent inclusion nanolayers, where the L2 systems exhibit higher PR value at $\sigma'/\sigma = 1.02$ than the L3 systems. In all cases, the auxetic properties are removed or significantly diminished for all systems, when $\sigma'/\sigma > 1.025$.

In Figures 6 and 7 the plots of the PR in spherical coordinates for C2 and C3 systems, respectively, have been presented. As described in Section III. 1. Poisson's ratio depends on the choice of two, mutually orthogonal directions. Two-dimensional plots in Fig. 5 give only limited insight in extreme values of four selected loading directions. It is not feasible to visualize in full the PR relation to these two angles. However, one can calculate the extreme values of Poisson's ratio at a given direction of applied load, and plot them as surfaces in the polar coordinates. For clarity, only the negative part of the surface of minimum PR has been plotted (in blue colour), to show the changes in the auxetic properties of the models. The red surfaces indicate the maximum PR with respect to different loading directions. All surfaces in each plot have been uniformly sampled in $4.5 \cdot 10^6$ different loading directions. Based on the investigation of the maximum PR, it can be seen that its increase occurs virtually for all n-directions, both in the case when the inclusion diameters increase and decrease, with respect to the matrix spheres. Here, it also can be noticed that this increase is more significant for high values of σ'/σ. When examining the surfaces of negative Poisson's ratio the conclusion from previous paragraph is confirmed. The auxetic properties are removed from all systems at higher values of σ'/σ and significantly diminished at low values of σ'/σ. However, what is interesting to note, depending on the size of the nanochannel, the auxetic properties are diminished in different directions. One can observe in Fig. 6 for the C2 models, that auxetic properties are very small in-plane, whereas the directions $[101]$, $[011]$ and their symmetric counterparts, still show a notable negative PR. On the other hand, for the C3 system (especially for C3L2) in Fig. 7, it can be seen that at $\sigma'/\sigma = 0.95$, the out-of-plane directions, mentioned above, show small to none auxetic properties, whereas for $[110]$ (in-plane) direction, PR is notably more negative. This can be attributed to the orientation of the nanochannel with respect

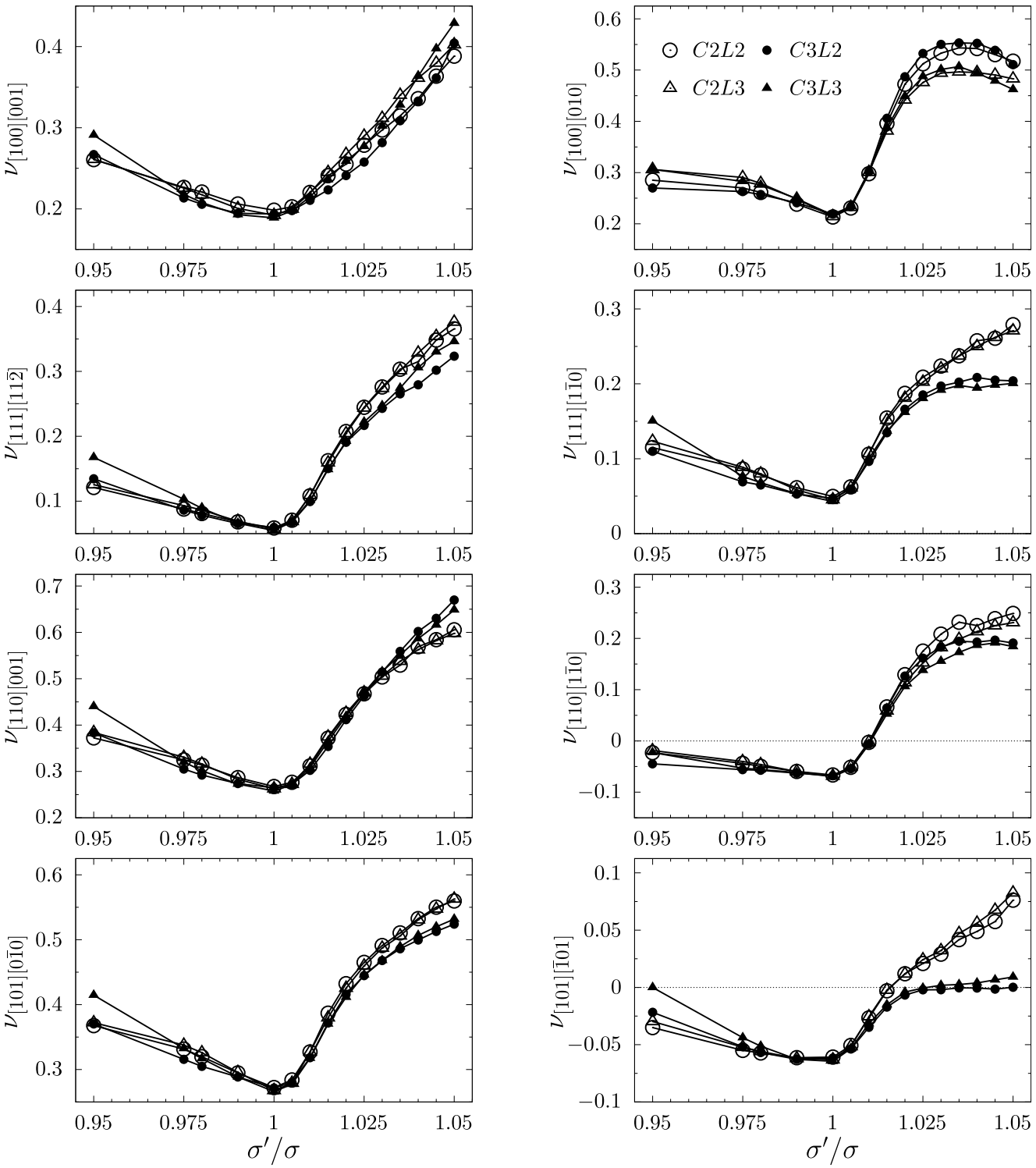

Fig. 5. Poisson's ratio (ν) in selected crystallographic directions for all studied systems plotted against the values of atomic diameter σ'/σ.

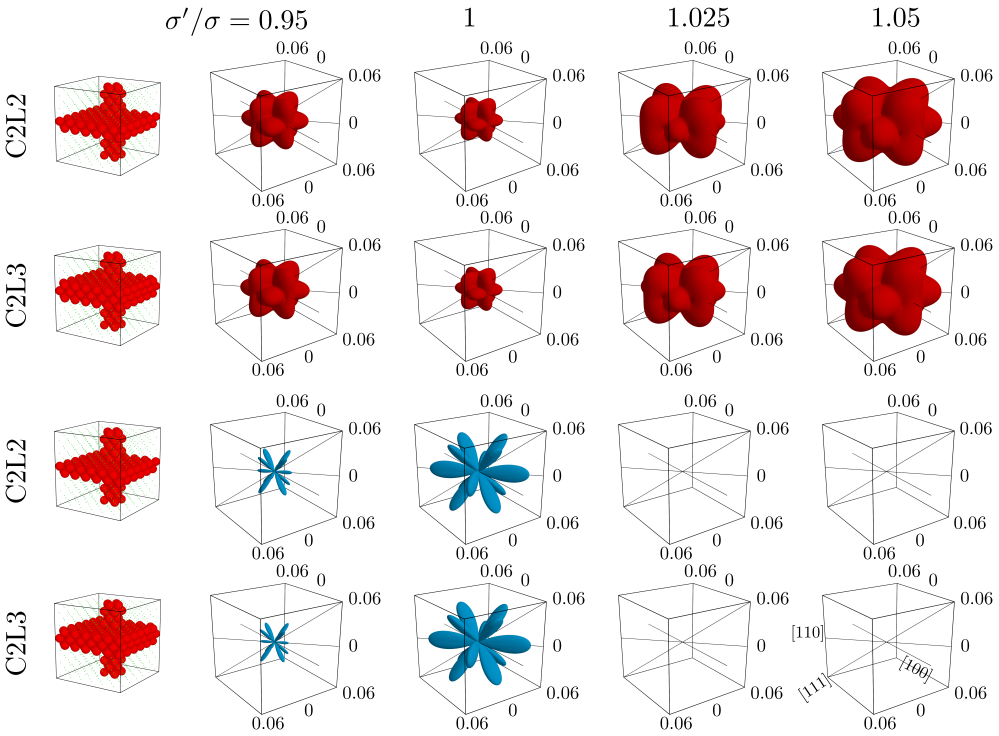

Fig. 6. The surface of the maximum Poisson's ratio (red) with respect to the loading direction $\vec{\mathbf{n}}$, and the negative part of the minimum Poisson's ratio surface (blue), plotted in the spherical coordinates for C2 systems at selected values of σ'/σ.

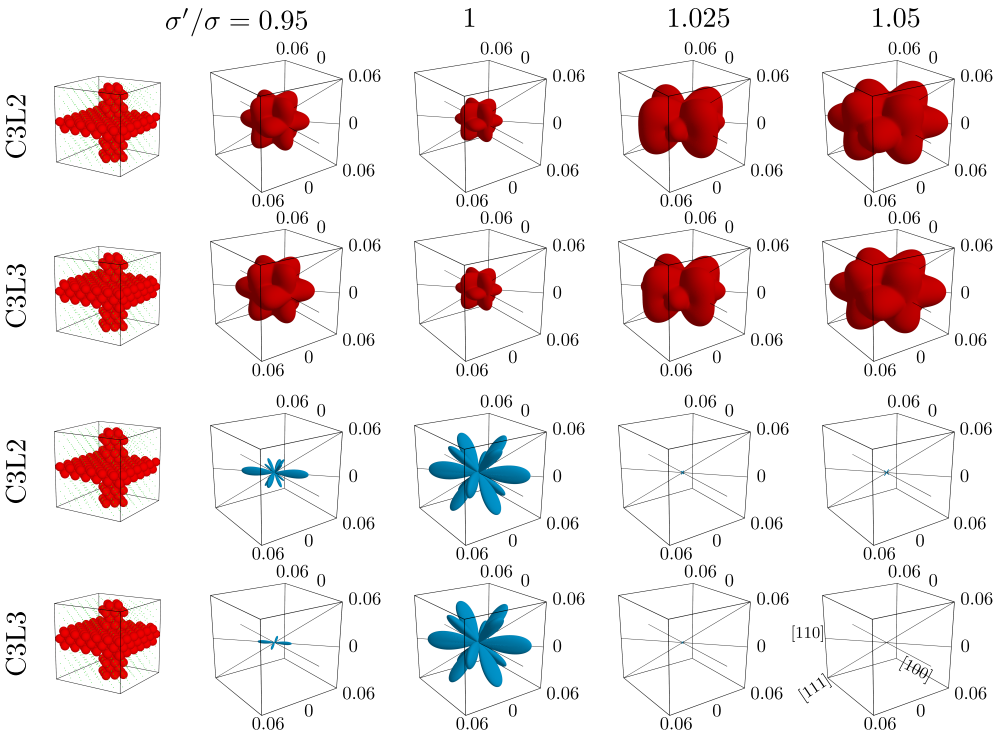

Fig. 7. The surface of the maximum Poisson's ratio (red) with respect to the loading direction $\vec{\mathbf{n}}$, and the negative part of the minimum Poisson's ratio surface (blue), plotted in the spherical coordinates for C3 systems at selected values of σ'/σ.

to the crystal. In both cases, C2 and C3 nanochannels occupy a cuboid space. The notable difference, when viewed from the [001]-direction, is that the C2 nanochannel sides are parallel to the respective sides of the cuboid described by the $\mathbf{h}$

matrix. Whereas in the case of the C3 nanochanel, the latter is rotated by $\pi/4$ around $[001]$-direction, which may explain the different behaviour of auxetic properties between the systems. Similar models, but containing only single nanolayer inclusions filled with dumbbells, have been recently studied [61], but in those systems the effect of increasing size of the nanochannel on switching the auxeticity between different directions when $\sigma'/\sigma < 1$, was very weak. Here, with multiple adjacent nanolayers and wider nanochannels, it is feasible to think about the possibility of applying this effect e.g. in nanoscale directional stress/strain sensors to detect in-plane or out-of-plane deformations.

V. Summary and Conclusions

The elastic properties of f.c.c. hard sphere crystal containing nanostructural inclusions, have been studied here with the computer simulations. Monte Carlo method in the NpT ensemble has been used to calculate the elastic properties of four different model crystals, containing different configurations of hybrid nanolayer and nanochannel inclusions, filled by simple di-atomic molecules, called dumbbells. The dumbbell molecules created the degenerate phase did not exhibit any periodic order of molecules within the inclusion. The diameters of spheres forming dumbbells were increased or decreased with respect to the diameters of spheres forming the matrix of the crystal. The impact of these changes of the inclusion particles sizes, along with the different configuration of the inclusion shapes and sizes, on elastic properties of the f.c.c. crystal, have been the subject of this study, which is an extension of the study done in [61]. It has been shown that adding multiple adjacent nanolayers filled with dumbbells is responsible for the removal of auxetic properties from the f.c.c. hard sphere crystal, when the diameter of inclusion spheres is at least $\sigma'/\sigma = 1.02$. It has been shown that, for most cases, values of PR in given directions weakly depend on the configuration of inclusions that have been studied. Only for $\nu_{[101][\bar{1}01]}$ and $\nu_{[111][1\bar{1}0]}$ a notable difference at high values of σ'/σ has been observed. Interestingly, changing the size of the nanochannel shows significant impact on the auxetic properties at low values of σ'/σ. It has been shown that different nanochannel sizes can remove or significantly diminish auxetic properties in either the in-plane or the out-of-plane directions. This effect might find applications e.g. in nanoscale sensors for detecting the direction of applied stress.

Acknowledgment

The computations were partially performed at Poznań Supercomputing and Networking Center (PCSS).

References

[1] L. D. Landau and E. M. Lifshitz. *Theory of Elasticity*. Pergamon Press, London, UK, 1986.

[2] R. S. Lakes. Foam structures with a negative Poisson's ratio. *Science*, 235: pp. 1038–1040, 1987.

[3] K. W. Wojciechowski. Constant thermodynamic tension Monte Carlo studies of elastic properties of a two-dimensional system of hard cyclic hexamers. *Mol. Phys.*, 61: pp. 1247–1258, 1987.

[4] K. W. Wojciechowski. Two-dimensional isotropic model with a negative Poisson ratio. *Phys. Lett. A*, 137: pp. 60–64, 1989.

[5] K. E. Evans. Auxetic polymers: a new range of materials. *Endeavour*, 15: pp. 170–174, 1991.

[6] K. E. Evans and A. Alderson. Auxetic materials: Functional materials and structures from lateral thinking! *Adv. Mater.*, 12: pp. 617–628, 2000.

[7] Y. Prawoto. Seeing auxetic materials from the mechanics point of view: A structural review on the negative Poisson's ratio. *Comput. Mater. Sci.*, 58: pp. 140–153, 2012.

[8] T.-C. Lim. *Mechanics of Metamaterials with Negative Parameters*. Springer: Singapore, 2020.

[9] J. B. Choi and R. S. Lakes. Design of a fastener based on negative poissons ratio foam. *Cellular Polymers*, 10(3): pp. 205–212, 1991.

[10] M. Kapnisi, C. Mansfield, C. Marijon, A. G. Guex, F. Perbellini, I. Bardi, E. J. Humphrey, J. L. Puetzer, D. Mawad, D. C. Koutsogeorgis, D. J. Stuckey, C. M. Terracciano, S. E. Harding, and M. M. Stevens. Auxetic cardiac patches with tunable mechanical and conductive properties toward treating myocardial infarction. *Adv. Funct. Mater.*, 28:1800618, 2018.

[11] A. Kasal, T. Kuskun, and J. Smardzewski. Experimental and numerical study on withdrawal strength of different types of auxetic dowels for furniture joints. *Materials*, 13(19):4252, 2020.

[12] D. Tahir, M. Zhang, and H. Hu. Auxetic materials for personal protection: A review. *Phys. Status Solidi B-Basic Solid State Phys.*, 259(12):2200324, 2022.

[13] R. F. Almgren. An isotropic three-dimensional structure with Poisson's ratio =-1. *J. Elast.*, 15: pp. 427–430, 1985.

[14] S. Bao, X. Ren, Y. J. Qi, H. R. Li, D. Han, W. Li, C. Luo, and Z. Z. Song. Quasi-static mechanical properties of a modified auxetic re-entrant honeycomb metamaterial. *Phys. Status Solidi B-Basic Solid State Phys.*, 259(12):2200270, 2022.

[15] H. Sun, H. Zhou, J. Zhang, L. Wang, and T. Wang. Multiple crashworthiness evaluation of double-v npr filled square tube under axial impact. *Phys. Status Solidi B-Basic Solid State Phys.*, 259(12):2200388, 2022.

[16] E. A. Korznikova, K. Zhou, L. Kh. Galiakhmetova, E. G. Soboleva, A. A. Kudreyko, and S. V. Dmitriev. Partial auxeticity of laterally compressed carbon nanotube bundles. *Phys. Status Solidi - Rapid Research Letters*, 16(1):2100189, 2022.

[17] N. Novak, M. Nowak, M. Vesenjak, and Z. Ren. Structural optimization of the novel 3d graded axisymmetric chiral auxetic structure. *Phys. Status Solidi B-Basic Solid State Phys.*, 259(12):2200409, 2022.

[18] T.-C. Lim. Auxetic and non-auxetic metamaterial model from interconnected rotating parallelograms and triangles. *Phys. Status Solidi B-Basic Solid State Phys.*, 261(12):2300413, 2024.

[19] P.-S. Farrugia, R. Gatt, and J. N. Grima. Creating a three-dimensional auxetic system using torsion springs. *Phys. Status Solidi B-Basic Solid State Phys.*, 261(12):2400212, 2024.

[20] T.-C. Lim. Auxetic metamaterial model made from rotating rectangles, hexagons, and triangles. *Phys. Status Solidi B-Basic Solid State Phys.*, Early view:2400343, 2025.

[21] O. Duncan, F. Clegg, A. Essa, A. M. T. Bell, L. Foster, T. Allen, and A. Alderson. Effects of heat exposure and volumetric compression on Poisson's ratios, Young's moduli, and polymeric composition during thermo-mechanical conversion of auxetic open cell polyurethane foam. *Phys. Status Solidi B-Basic Solid State Phys.*, 256(1):1800393, 2019.

[22] S. Mohsenizadeh, Z. Ahmad, R. Alipour, R. A. Majid, and Y. Prawoto. Quasi tri-axial method for the fabrication of optimized polyurethane auxetic foams. *Phys. Status Solidi B-Basic Solid State Phys.*, 256(10):1800587, 2019.

[23] O. Duncan, A. Alderson, and T. Allen. Fabrication, characterization and analytical modeling of gradient auxetic closed cell foams. *Smart Mater. Struct.*, 30(3):035014, 2021.

[24] Q. Zhang, X. Yu, Y. Xia, D. Zhang, R. S. Lakes, K. W. Wojciechowski, and F. Scarpa. The shear performance of uniaxially thermoformed auxetic polymer foams. *Composites Part B*, 286: 111791, 2024.

[25] A. Zulifqar, T. Hua, and H. Hu. Single- and double-layered bistretch auxetic woven fabrics made of nonauxetic yarns based on foldable geometries. *Phys. Status Solidi B-Basic Solid State Phys.*, 257(10):1900156, 2020.

[26] S. Zhao, Y. Chang, Y. Yang, H. Kamrul, M. Zhang, and H. Hu. Deformation behaviors of auxetic warp knitted fabrics based on reentrant geometry. *Phys. Status Solidi B-Basic Solid State Phys.*, 258(12):2000580, 2021.

[27] Y. Chang and H. Hu. 3d fabrics with negative poisson's ratio: A review. *Applied Composite Materials*, 29: pp. 95–108, 2022.

[28] D. M. Kochmann and G. N. Venturini. Homogenized mechanical properties of auxetic composite materials in finite-strain elasticity. *Smart Mater. Struct.*, 22:084004, 2013.

[29] I. Shufrin, E. Pasternak, and A. V. Dyskin. Effective properties of layered auxetic hybrids. *Composite Structures*, 209: pp. 391–400, 2019.

[30] N. Novak, M. Vesenjak, G. Kennedy, N. Thadhani, and Z. Ren. Response of chiral auxetic composite sandwich panel to fragment simulating projectile impact. *Phys. Status Solidi B-Basic Solid State Phys.*, 257(10):1900099, 2020.

[31] F. Portone, M. Amorini, M. Montanari, R. Pinalli, A. Pedrini, R. Verucchi, R. Brighenti, and E. Dalcanale. Molecular auxetic polymer of intrinsic microporosity via conformational switching of a cavitand crosslinker. *Advanced Functional Materials*, 33(51):2307605, 2023.

[32] K. Bertoldi, V. Vitelli, J. Christensen, and M. van Hecke. Flexible mechanical metamaterials. *Nature Reviews Materials*, 2:17066, 2017.

[33] Y. Y. Chen, T. T. Li, F. Scarpa, and L. F. Wang. Lattice metamaterials with mechanically tunable Poisson's ratio for vibration control. *Physical Review Applied*, 7: 024012, 2017.

[34] K. K. Dudek, J. A. I. Martinez, G. Ulliac, and M. Kadic. Micro-scale auxetic hierarchical mechanical metamaterials for shape morphing. *Advanced Materials*, 34(14):2110115, 2022.

[35] K. K. Dudek, J. A. I. Martinez, G. Ulliac, L. Hirsinger, L. Wang, V. Laude, and M. Kadic. Micro-scale mechanical metamaterial with a controllable transition in the Poisson's ratio and band gap formation. *Advanced Materials*, 35:2210993, 2023.

[36] R. Galea Mifsud, K. K. Dudek, P.-S. Farrugia, J. N. Grima, and R. Gatt. Egg-rack-like active magnetomechanical metamaterial. *Phys. Status Solidi B-Basic Solid State Phys.*, Early view:2400528, 2025.

[37] J. N. Grima and K. E. Evans. Auxetic behavior from rotating squares. *J. Mater. Sci. Lett.*, 19: pp. 1563–1565, 2000.

[38] Wm. G. Hoover and C. G. Hoover. Searching for auxetics with DYNA3D and ParaDyn. *Phys. Status Solidi B-Basic Solid State Phys.*, 242(3): pp. 585–594, 2005.

[39] R. V. Goldstein, V. A. Gorodtsov, and D. S. Lisovenko. The elastic properties of hexagonal auxetics under pressure. *Phys. Status Solidi B-Basic Solid State Phys.*, 253(7): pp. 1261–1269, 2016.

[40] R. V. Goldstein, V. A. Gorodtsov, D. S. Lisovenko, and M. A. Volkov. Auxeticity in nano/microtubes produced from orthorhombic crystals. *Smart Mater. Struct.*, 25(5):05006, 2016.

[41] R. V. Goldstein, V. A. Gorodtsov, and D. S. Lisovenko. Longitudinal elastic tension of two-layered plates from isotropic auxetics-nonauxetics and cubic crystals. *European Journal of Mechanics A-Solids*, 63:pp. 122–127, 2017.

[42] K. K. Dudek, R. Gatt, L. Mizzi, M. R. Dudek, D. Attard, K. E. Evans, and J. N. Grima. On the dynamics and control of mechanical properties of hierarchical rotating rigid unit auxetics. *Sci Rep*, 7: 46529, 2017.

[43] V. A. Gorodtsov, M. A. Volkov, and D. S. Lisovenko. Out-of-plane tension of thin two-layered plates of cubic crystals. *Phys. Status Solidi B-Basic Solid State Phys.*, 258(12):2100184, 2021.

[44] S. Czarnecki and T. Łukasiak. Auxetic properties of the stiffest elastic bodies as a result of topology optimization and microstructures recovery based on homogenization method. *Phys. Status Solidi B-Basic Solid State Phys.*, 261(12):2300495, 2024.

[45] R. H. Baughman, J. M. Shacklette, A. A. Zakhidov, and S. Stafstrom. Negative Poisson's ratios as a common feature of cubic metals. *Nature*, 392: pp. 362–365, 1998.

[46] A. C. Brańka, D. M. Heyes, and K. W. Wojciechowski. Auxeticity of cubic materials under pressure. *Phys. Status Solidi B-Basic Solid State Phys.*, 248: pp. 96–104, 2011.

[47] K. V. Tretiakov and K. W. Wojciechowski. Poisson's ratio of simple planar 'isotropic' solids in two dimensions. *Phys. Status Solidi B-Basic Solid State Phys.*, 244(3): pp. 1038–1046, 2007.

[48] K. V. Tretiakov. Negative Poisson's ratio of two-dimensional hard cyclic tetramers. *J. Non-Cryst. Solids*, 355: pp. 1435–1438, 2009.

[49] P. Kolat, B. M. Maruszewski, and K. W. Wojciechowski. Solitary waves in auxetic plates. *Journal of Non-Crystalline Solids*, 356(37-40): pp. 2001–2009, 2010.

[50] K. V. Tretiakov and K. W. Wojciechowski. Auxetic, partially auxetic, and nonauxetic behaviour in 2D crystals of hard cyclic tetramers. *Phys. Status Solidi-Rapid Res. Lett.*, 14: 2000198, 2020.

[51] K. V. Tretiakov and K. W. Wojciechowski. Auxeticity and its pressure dependence for strongly anisotropic hard cyclic tetramers. *Phys. Status Solidi-Rapid Res. Lett.*, page 2200288, 2022.

[52] R. Ali, M. R. Saleem, M. Roussey, J. Turunen, and S. Honkanen. Fabrication of buried nanostructures by atomic layer deposition. *Scientific Reports*, 8: 15098, 2018.

[53] K. V. Tretiakov, P. M. Piglowski, K. Hyzorek, and K. W. Wojciechowski. Enhanced auxeticity in Yukawa systems due to introduction of nanochannels in [001]-direction. *Smart Mater. Struct.*, 25:054007, 2016.

[54] J. W. Narojczyk, K. W. Wojciechowski, K. V. Tretiakov, J. Smardzewski, F. Scarpa, P. M. Piglowski, M. Kowalik, A. R. Imre, and M. Bilski. Auxetic properties of a f.c.c. crystal of hard spheres with an array of $[001]$-nanochannels filled by hard spheres of another diameter. *Phys. Status Solidi B-Basic Solid State Phys.*, 256: 1800611, 2019.

[55] J. W. Narojczyk and K. W. Wojciechowski. Poisson's ratio of the f.c.c. hard sphere crystals with periodically stacked (001)-nanolayers of hard spheres of another diameter. *Materials*, 12: 700, 2019.

[56] J. W. Narojczyk, K. W. Wojciechowski, J. Smardzewski, A. R. Imre, J. N. Grima, and M. Bilski. Cancellation of auxetic properties in f.c.c. hard sphere crystals by hybrid layer-channel nanoinclusions filled by hard spheres of another diameter. *Materials*, 14: 3008, 2021.

[57] J. W. Narojczyk. Increase in auxeticity due to the presence of a disordered crystalline phase of hard dumbbells within the nanolayer–nanochannel inclusion introduced to the f.c.c. hard sphere crystal. *Materials*, 17:5558, 2024.

[58] K. W. Wojciechowski, D. Frenkel, and A. C. Brańka. Nonperiodic solid phase in a two-dimensional hard-dimer system. *Phys. Rev. Lett.*, 66: pp. 3168–3171, 1991.

[59] K. W. Wojciechowski, A. C. Brańka, and D. Frenkel. Monte Carlo simulation of a two-dimensional hard dimer system. *Physica A*, 196: pp. 519–545, 1993.

[60] K. W. Wojciechowski. Solid phases of two-dimensional hard dumb-bells in the free volume approximation: crystal-aperiodic-solid phase transition. *Phys. Lett. A*, 122(6-7): pp. 377–380, 1987.

[61] J. W. Narojczyk, K. V. Tretiakov, J. Smardzewski, F. Scarpa, and K. W. Wojciechowski. Elastic properties of the fcc hard sphere crystal with nanolayer–nanochannel inclusions formed by the aperiodic crystalline phase of hard dumbbells. *Phys. Status Solidi B-Basic Solid State Phys.*, 263(5), 2026. submitted.

[62] J. P. Hansen and I. R. McDonald. *Theory of Simple Liquids*. Academic Press, Amsterdam, The Netherlands, 2006.

[63] M. P. Allen and D. J. Tildesley. *Computer Simulations of Liquids*. Clarendon Press, Oxford, UK, 1987.

[64] K. J. Runge and G. V. Chester. Monte Carlo determination of the elastic constants of the hard-sphere solid. *Phys. Rev. A*, 36: pp. 4852–4858, 1987.

[65] K. V. Tretiakov and K. W. Wojciechowski. Elastic properties of soft sphere crystal from Monte Carlo simulations. *J. Phys. Chem. B*, 112: pp. 1699–1705, 2008.

[66] M. Parrinello and A. Rahman. Polymorphic transitions in single crystals: A new molecular dynamics method. *J. Appl. Phys.*, 52: pp. 7182–7190, 1981.

[67] M. Parrinello and A. Rahman. Strain fluctuations and elastic constants. *J. Chem. Phys.*, 76: pp. 2662–2666, 1982.

[68] K. W. Wojciechowski, K. V. Tretiakov, and M. Kowalik. Elastic properties of dense solid phases of hard cyclic pentamers and heptamers in two dimensions. *Phys. Rev. E*, 67: 036121, 2003.

[69] J. H. Weiner. *Statistical Mechanics of Elasticity*. Wiley, New York, USA, 1983.

[70] S. P. Tokmakova. Stereographic projections of Poisson's ratio in auxetic crystals. *Phys. Status Solidi B-Basic Solid State Phys.*, 242(3): pp. 721–729, 2005.

[71] J. F. Nye. *Physical Properties of Crystals, Their Representation by Tensors and Matrices*. Clarendon Press, Oxford, UK, 1957.

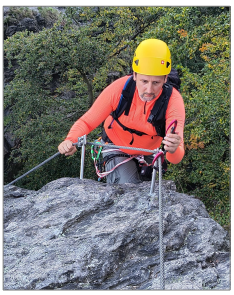

Jakub W. Narojczyk received his PhD from the Institute of Molecular Physics of the Polish Academy of Sciences (IMP PAS) in Poznań. Recently he received habilitation from IMP PAS for his work on elastic properties of hard sphere models. He is a computational physicist with a strong background in Monte Carlo and Molecular Dynamics simulation methods. He has in-depth knowledge of C programming language and a solid experience in administration of GNU/Linux class operating systems as well as High-Performance Computing environment. He works as an Assistant Professor in the IMP PAS, where he conducts research (by means of computer simulations) on elastic properties of model materials, with emphasis on their Poisson's ratio. The research is aimed at the search for systems for which the Poisson's ratio takes negative values (such materials are called auxetics) as well as mechanisms and phenomena responsible for the decrease of the Poisson's ratio of materials. Currently, his studies are focused on the influence of various forms of nanoinclusions in the atomic structure on the elastic properties of various model systems. He guest co-edited one special issue of Physica Status Solidi B and four abstract books from the conferences on Auxetics and Related Systems. He is a peer reviewer for various scientific journals including Applied Physics Letters, Applied Sciences, Advanced Theory and Simulations, Carbon, Materials and Design, Physica Status Solidi B, and Computational Methods in Science and Technology.

Konstantin V. Tretiakov is a Full Professor at the Institute of Molecular Physics of the Polish Academy of Sciences (IMP PAS) in Poznań and at President Stanisław Wojciechowski University of Kalisz. He is Head of the Group of Auxetics, Functional Materials, and Computer Simulations at the Institute of Molecular Physics of the Polish Academy of Sciences in Poznań. He graduated summa cum laude in Industrial Electronics from the Pavel Sukhoi State Technical University (Gomel, Belarus) in 1994. He received his PhD in Physics from the Institute of Molecular Physics, Polish Academy of Sciences (Poznan, Poland) in 2000. From 2002 to 2004, Dr. Tretiakov was a Postdoctoral Fellow in the Condensed Matter and Statistical Physics Section at the Abdus Salam International Center for Theoretical Physics (Trieste, Italy). From 2007 to 2009, Dr. Tretiakov worked in the Department of Chemical and Biological Engineering at Northwestern University (Evanston, USA). He prepared his habilitation in 2011. Since 2014, he has been an Associate Professor at the Institute of Molecular Physics of the Polish Academy of Sciences. According to the decision of the President of the Republic of Poland dated March 18, 2024, he has been appointed a full professor of natural sciences in the physical sciences. Professor Tretiakov specializes in statistical physics and computer simulation of many-body systems, with research focusing on non-equilibrium self-assembling systems, transport properties of soft matter, and the elastic properties of solids, particularly those exhibiting a negative Poisson's ratio. He is a member of the Editorial Board of the CMST.

Krzysztof Witold Wojciechowski is a Full Professor at the Institute of Molecular Physics of the Polish Academy of Sciences (IMP PAS) in Poznań. He headed there the Department of Nonlinear Dynamics and Computer Simulations and the Division of Soft Matter Physics and Functional Materials for about 25 and 10 years, respectively. He received the MSc degree with honors in Theoretical Physics (liquid crystals) and the MSc degree in Mathematics (applications of Noether theorem in physics) from the Adam Mickiewicz University in Poznań. He earned the PhD in Physics (quasi-one-dimensional systems) from the IMP PAS, where he also habilitated in computer simulations. By the decision of the President of Poland, he obtained the title of Professor of the physical sciences. He was a holder of scholarships at SISSA and ICTP (Trieste, Italy), FOM-AMOLF (Amsterdam, Netherlands), and CINECA (Bologna, Italy). His research interests concern, among other topics, statistical mechanics of hard-body systems, algorithms for simulations of many-body systems, auxetics and influence of various mechanisms on the Poisson's ratio of condensed matter systems, materials with unstable inclusions, generators of (pseudo)random numbers, applications of fractional derivative in physics, and exotic liquid crystalline phases. He is a (co-)author of more than 200 research papers written in English, Polish or Russian and published in such journals as Phys. Rev. Lett., Advanced Materials, Composites Part B, Phys. Lett. A, Phys. Rev. A, Phys. Rev. B, Phys. Rev. E, J. Chem. Phys., J. Phys. Chem. A, Molecular Physics, Materials, etc. Prof. Wojciechowski guest co-edited more than two dozen thematic issues (on auxetics and related materials, mechanics of continuous media, statistical mechanics of condensed matter, computer simulation methods, nonlinear and disordered systems) for international journals including J. Mech. Mat. Struct. (2), J. Non-Cryst. Solids (4), Phys. Status Solidi B (16), Rev. Adv. Mat. Sci. (2), Smart Materials and Structures (2), etc. He is the co-Editor of CMST (OWN, PL) and a member of the Editorial Board of Smart Materials and Structures (IOP Publishing, UK) and TASK Quarterly (TASK, PL). He is a regular name in all the Stanford/Elsevier's Top 2% Scientist Rankings. In 2015, the President of the Republic of Poland awarded Prof. Wojciechowski the Knight's Cross of the Order of Polonia Restituta.